

Hindered Coulomb explosion of embedded Na clusters – stopping, shape dynamics and energy transport

F. Fehrer¹, P.M. Dinh², M. Bär¹, P.-G. Reinhard², and E. Suraud¹

¹ Laboratoire de Physique Théorique, Université P. Sabatier, 118 Rte de Narbonne, F-31062 Toulouse cedex, France

² Institut für Theoretische Physik, Universität Erlangen, Staudtstrasse 7, D-91058 Erlangen, Germany

November 12, 2018/ Received: date / Revised version: date

Abstract. We investigate the dynamical evolution of a Na₈ cluster embedded in Ar matrices of various sizes from $N = 30$ to 1048. The system is excited by an intense short laser pulse leading to high ionization stages. We analyze the subsequent highly non-linear motion of cluster and Ar environment in terms of trajectories, shapes, and energy flow. The most prominent effects are : temporary stabilization of high charge states for several ps, sudden stopping of the Coulomb explosion of the embedded Na₈ clusters associated with an extremely fast energy transfer to the Ar matrix, fast distribution of energy throughout the Ar layers by a sound wave. Other ionic-atomic transfer and relaxation processes proceed at slower scale of few ps. The electron cloud is almost thermally decoupled from ions and thermalizes far beyond the ps scale.

PACS. 36.40.Gk, 36.40.Mr, 36.40.Sx, 36.40.Vz, 61.46.Bc Atomic and molecular clusters

1 Introduction

Metal clusters have many interesting properties which made them a much studied species in the past decades. Their valence electron cloud provides a finite fermion system with remarkable properties as electronic shell effects and strong optical absorption in a narrow frequency band, the Mie surface-plasmon resonance, for early reviews see [1, 2, 3]. The resonance depends sensitively on the geometry of the cluster and thus provides an ideal handle for analyzing and for controlling cluster dynamics. This has been much exploited for free clusters in all dynamical regimes, for a recent overview see [4].

The dynamical scenarios become more involved when clusters stay in contact with a substrate, either embedded inside or deposited on a surface. The variety of combinations grows huge. This is generally viewed as an advantage because it allows to tailor desired properties, e.g., for designing bio-markers exploiting the prominent optical properties of clusters [5, 6]. Corresponding to the huge manifold of possibilities, there is a huge body of publications. But comparatively little has been done yet in the regime of highly non-linear dynamics induced by intense laser fields.

It is the aim of the present contribution to explore, from a theoretical perspective, that non-linear regime. As test case, we take Na clusters because these are conceptually the cleanest metal clusters, least plagued by interference with core electrons and also the simplest for a theoretical description. The clusters are embedded in an Ar substrate. This is an insulator and so we simulate a typ-

ical scenario for a chromophore in an inert environment. Moreover, Ar is a very soft material having a weak interface energy. It exerts only a very small perturbation on the cluster which, in turn, maintains basically its structure and optical properties. That feature had been exploited in the past for studying optical properties of neutral clusters which are otherwise hard to handle as free clusters, see e.g. [7, 8]. The weak-perturbative situation will change if we consider violent dynamics where cluster electrons and ions are driven to heftier encounters with the surrounding substrate atoms. The actual test case will be Na₈ embedded in a sufficiently large cavity of the Ar_N system. We will consider various Ar system sizes N . This serves a double purpose : large N serve as an approximation to bulk Ar and comparison with smaller N allows to work out typical effects of mixed clusters, which are as such an interesting species. We excite the embedded cluster by intense and short laser pulses to high charge states (Na₈^{Q+} up to $Q = 4$) and follow the subsequent dynamical evolution over up to 8 ps. We will analyze the results in terms of detailed views, energy transfers, evolution of global shape, and relaxation times.

Clusters in contact with a substrate are much more complex systems than free clusters. The expense for a fully detailed theoretical description grows huge. Such calculations are undertaken where details count, mostly for studying structure of small compounds (see e.g [9, 10, 11] for deposited and embedded metal clusters in various material combinations). But these subtle models are hardly applicable to a truly dynamical situation and the enor-

mous effort is not really needed for the sort of exploratory studies which we have in mind here. The large difference between metal clusters (reactive) and rare gas (inert) suggests a hierarchical model where the environment is handled at a lower level of description. Such approaches are widely used in theoretical chemistry under the label Quantum-Mechanical/Molecular-Mechanical model (QM/MM), see e.g. [12], and in surface physics, see e.g., [13]. A model in that spirit for Na clusters in contact with Ar was proposed in [14] and applied to structure, optical response and moderately non-linear dynamics of embedded clusters in [15,16]. Here we are going to carry forth the studies in the regime of strong laser excitations inducing high charge states and large rearrangements of cluster and matrix structure.

2 Formal framework

2.1 Short summary of the model

In order to allow for a sufficiently large Ar matrix, we use a hierarchical approach. We sketch it here briefly and refer to [14,17] for a detailed layout.

The Na cluster is treated in full microscopic detail using quantum-mechanical single-particle wavefunctions $\{\varphi_n(\mathbf{r}, t), n = 1, \dots, N_{\text{el}}\}$ for the valence electrons. These are coupled non-adiabatically to classical molecular dynamics (MD) for the Na^+ ions which are described by their positions $\{\mathbf{R}_I, I = 1, \dots, N_{\text{Na}}\}$. In the present paper, we have $N_{\text{el}} = N_{\text{Na}} = 8$. The electronic wavefunctions are propagated by time-dependent local-density approximation (TDLDA). The electron-ion interaction in the cluster is described by soft, local pseudo-potentials. This TDLDA-MD has been widely validated for linear and non-linear dynamics of free metal clusters [4,18].

Two classical degrees-of-freedom are associated with each Ar atom : center-of-mass $\{\mathbf{R}_a, a = 1, \dots, N\}$, and electrical dipole moment which is parameterized as $\{\mathbf{R}'_a = \mathbf{R}_a + \mathbf{d}_a, a = 1, \dots, N\}$. Note that the Ar dipole is practically handled by two constituents with opposite charge, positive Ar core (at \mathbf{R}_a) and negative Ar valence cloud (at \mathbf{R}'_a). With the atomic dipoles, we explicitly treat the dynamical polarizability of the atoms through polarization potentials [19]. Smooth, Gaussian charge distributions are used for Ar ionic cores and electron clouds in order to regularize the singular dipole interaction. We associate a Gaussian charge distribution to both constituents having a width of the order of the 3p shell in Ar, similar as was done in [20]. The Coulomb field of the (softened) Ar dipoles provides the polarization potentials which are the dominant agents at long range. The Na^+ ions of the metal cluster have net charge $q_{\text{Na}} = +1$ and interact with the Ar dipoles predominantly by the monopole moment. The small dipole polarizability of the Na^+ core is neglected. The cluster electrons do also couple naturally to the Coulomb field generated by the atoms.

The model is fully specified by giving the total energy of the system. It is composed as

$$E_{\text{total}} = E_{\text{Nacluster}} + E_{\text{Ar}} + E_{\text{coupl}} + E_{\text{VdW}} \quad (1)$$

The energy of the Na cluster $E_{\text{Nacluster}}$ consists of TDLDA (with a self-interaction correction, see Sec. 2.2) for the electrons, MD for ions, and a coupling of both by soft, local pseudo-potentials; that standard treatment is well documented at many places, e.g. [4,18]. The Ar system and its coupling to the clusters are described by

$$E_{\text{Ar}} = \sum_a \frac{\mathbf{P}_a^2}{2M_{\text{Ar}}} + \sum_a \frac{\mathbf{P}'_a{}^2}{2m_{\text{Ar}}} + \frac{1}{2}k_{\text{Ar}}(\mathbf{R}'_a - \mathbf{R}_a)^2 + \sum_{a < a'} \left[\int d\mathbf{r} \rho_{\text{Ar},a}(\mathbf{r}) V_{\text{Ar},a'}^{(\text{pol})}(\mathbf{r}) + V_{\text{ArAr}}^{(\text{core})}(\mathbf{R}_a - \mathbf{R}_{a'}) \right], \quad (2)$$

$$E_{\text{coupl}} = \sum_{I,a} \left[V_{\text{Ar},a}^{(\text{pol})}(\mathbf{R}_I) + V'_{\text{NaAr}}(\mathbf{R}_I - \mathbf{R}_a) \right] + \int d\mathbf{r} \rho_{\text{el}}(\mathbf{r}) \sum_a \left[V_{\text{Ar},a}^{(\text{pol})}(\mathbf{r}) + W_{\text{elAr}}(|\mathbf{r} - \mathbf{R}_a|) \right] \quad (3)$$

$$V_{\text{Ar},a}^{(\text{pol})}(\mathbf{r}) = e^2 q_{\text{Ar}} \left[\frac{\text{erf}(|\mathbf{r} - \mathbf{R}_a|/\sigma_{\text{Ar}})}{|\mathbf{r} - \mathbf{R}_a|} - \frac{\text{erf}(|\mathbf{r} - \mathbf{R}'_a|/\sigma_{\text{Ar}})}{|\mathbf{r} - \mathbf{R}'_a|} \right], \quad (4)$$

$$W_{\text{elAr}}(r) = e^2 \frac{A_{\text{el}}}{1 + e^{\beta_{\text{el}}(r - r_{\text{el}})}}, \quad (5)$$

$$V_{\text{ArAr}}^{(\text{core})}(R) = e^2 A_{\text{Ar}} \left[\left(\frac{R_{\text{Ar}}}{R} \right)^{12} - \left(\frac{R_{\text{Ar}}}{R} \right)^6 \right], \quad (6)$$

$$V'_{\text{ArNa}}(R) = e^2 \left[A_{\text{Na}} \frac{e^{-\beta_{\text{Na}} R}}{R} - \frac{2}{1 + e^{\alpha_{\text{Na}}/R}} \left(\frac{C_{\text{Na},6}}{R^6} + \frac{C_{\text{Na},8}}{R^8} \right) \right], \quad (7)$$

$$4\pi \rho_{\text{Ar},a} = \Delta V_{\text{Ar},a}^{(\text{pol})}, \quad (8)$$

$$E_{\text{VdW}} = \frac{e^2}{2} \sum_a \alpha_a \left[\frac{(\int d\mathbf{r} \mathbf{f}_a(\mathbf{r}) \rho_{\text{el}}(\mathbf{r}))^2}{N_{\text{el}}} - \int d\mathbf{r} \mathbf{f}_a(\mathbf{r})^2 \rho_{\text{el}}(\mathbf{r}) \right], \quad (9)$$

$$\mathbf{f}_a(\mathbf{r}) = \nabla \frac{\text{erf}(|\mathbf{r} - \mathbf{R}_a|/\sigma_{\text{Ar}})}{|\mathbf{r} - \mathbf{R}_a|}, \quad (10)$$

$$\text{erf}(r) = \frac{2}{\sqrt{\pi}} \int_0^r dx e^{-x^2} \quad (11)$$

The calibration of the various contributions is taken from independent sources, except eventually for a final fine tuning to the NaAr dimer modifying only the term W_{elAr} of Eq.(5). The parameters are summarized in table 1. The third column of the table indicates the source for the parameters. In the following, we report briefly the motivations for the choices.

$V_{Ar,a}^{(pol)}$	$q_{Ar} = \frac{\alpha_{Ar} m_{el} \omega_0^2}{e^2}$, $k_{Ar} = \frac{e^2 q_{Ar}^2}{\alpha_{Ar}}$, $m_{Ar} = q_{Ar} m_{el}$, $\sigma_{RG} = \left(\alpha_{Ar} \frac{4\pi}{3(2\pi)^{3/2}} \right)^{1/3}$	$\alpha_{Ar} = 11.08 \text{ a}_0^3$ $\omega_0 = 1.755 \text{ Ry}$
W_{elAr}	$A_{el} = 0.47$, $\beta_{el} = 1.6941 / \text{a}_0$, $r_{el} = 2.2 \text{ a}_0$	fit to NaAr dimer
$V_{ArAr}^{(core)}$	$A_{Ar} = 1.367 \times 10^{-3} \text{ Ry}$, $R_{Ar} = 6.501 \text{ a}_0$	fit to bulk Ar
V'_{ArNa}	$\beta_{Na} = 1.7624 \text{ a}_0^{-1}$, $\alpha_{Na} = 1.815 \text{ a}_0$, $A_{Na} = 334.85$, $C_{Na,6} = 52.5 \text{ a}_0^6$, $C_{Na,8} = 1383 \text{ a}_0^8$	after [21]

Table 1. Parameters for the various model potentials. See text for detail.

Most important are the polarization potentials defined in Eq.(4). They are described by the model of a valence electron cloud oscillating against the rare gas core ion. Their parameters are : q_{Ar} the effective charge of valence cloud, $m_{Ar} = q_{Ar} m_{el}$ the effective mass of valence cloud, k_{Ar} the restoring force for dipoles, and σ_{Ar} the width of the core and valence clouds. The q_{Ar} and k_{Ar} are adjusted to reproduce the dynamical polarizability $\alpha_D(\omega)$ of the Ar atom at low frequencies, i.e. we choose to reproduce the static limit $\alpha_D(\omega=0)$ and its second derivative $\alpha''_D(\omega=0)$. The width σ_{Ar} is determined consistently such that the restoring force from the folded Coulomb force (for small displacements) reproduces the spring constant k_{Ar} .

The short range repulsion is provided by the various core potentials. For the Ar-Ar core interaction, Eq.(6), we employ a Lennard-Jones type potential with parameters such that binding properties of bulk Ar are reproduced. The Na-Ar core potential Eq.(7) is chosen according to [21]. Note that the Na-Ar potential from [21] does also contain a long range part $\propto \alpha_{Ar}$ which accounts for the dipole polarization-potential. Since we describe that long range part explicitly, we have to omit it here. We thus choose the form as given in V'_{ArNa} .

The pseudo-potential W_{elAr} , Eq.(5), for the electron-Ar core repulsion has been modeled according to the proposal of [20]. Its parameters determine sensitively the binding properties of Na to the Ar atoms. We use them as a means for a final fine-tuning of the model. The benchmark for adjustment is provided by the Na-Ar dimer. The data (dimer binding energy, bond length, excitation energy) are taken from [22,23]. The adjustment shows some freedom in the choice of A_{el} . We exploit that to produce the softest reasonable core potential.

The Van-der-Waals energy, E_{vdW} , Eq.(9) stems from a correlation of the dipole excitation in the Ar atom coupled with a dipole excitation in the cluster. We exploit that the plasmon frequency ω_{Mie} is far below the excitations in the Ar atom. This simplifies the term to the variance of the dipole operator in the cluster, using again the regularized dipole operator \mathbf{f}_a corresponding to the smoothed Ar charge distributions.

2.2 Validity and limitations

A few words are in order about the range of validity for that hierarchical model. The structure of the coupled systems is well described by construction, see the predecessor in [20] and the extensive testing in [14]. The same holds for optical response (see [15,24]). However, one has to remain aware that the model has limitations with respect to allowed frequencies and amplitudes. The dynamical response of the Ar atoms is tuned to frequencies safely below the Ar resonance peak, i.e. safely below 15 eV. This is well fulfilled in the present calculations where the highest relevant frequency is the cluster's Mie plasmon at around 3 eV. The amplitudes of the dipole oscillations in Ar should also stay below the threshold where free electrons are released from the Ar atom into the matrix. That could become critical for the violent processes studied here. We checked the threshold for electron emission by fully quantum mechanical calculations of laser excitation on Ar atoms and we find a critical field strength of order of 1.4 eV/a₀. That value holds for constant fields. The case is more forgiving if the critical field strength is exceeded only for a short time. Anyway, we protocol during our calculation the actual field strength at each Ar site. We are on the safe side for the cases with charge $Q = 3$ and lower. The dynamics with charge $Q = 4$ shows occasionally field peaks above the limit, however for very short times.

The quantum mechanical treatment of the Na cluster involves two approximations which may limit the quantitative value of the results. The electron cloud is treated with axially averaged potentials and the TDLDA is augmented by a self-interaction correction (SIC) at the level of average-density SIC (ADSIC) [25,26]. Both approximations enhance the barriers for fragmentation of the cluster, or pieces thereof. The axial approximation is needed to enable the large scale calculations performed here. The SIC is compulsory for an appropriate description of ionization. We pay the price that our calculations provide rather a qualitative picture. The effects shown are certainly relevant. The thresholds concerning charge state and laser field strength are probably not too precise. However we also dispose of a full three-dimensional treatment for the valence electrons which, moreover, can handle various lev-

els of SIC and even exact exchange. We used that for occasional counterchecks and we never found significant (i.e. qualitative) deviations from the approximate treatment.

2.3 Initialization and propagation

The test cases in the following studies are Na_8 as free cluster and embedded in Ar_N where $N = 30, 164, 434,$ and 1048 . The Ar structures contain a cavity equivalent to 13 Ar places. This was found to provide sufficient space for convenient embedding of Na_8 . The latter consists of two rings carrying 4 Na ions each. The rings have the same diameter and are twisted by 45° relative to each other in order to minimize Coulomb energy. That structure is the same in all cases. The effect of the Ar surroundings on the structure is very small. For more details on structure and basic optical properties see [15]. All calculations start from fully relaxed stationary ground state configurations. A laser field is applied as time dependent dipole field with frequency $\omega_{\text{laser}} = 2 \text{ eV}$ and a temporal \sin^2 envelope with full width at half maximum (FWHM) of 33 fs. The intensity (\equiv field strength) is varied to reach the different final charge states $Q = 2, 3,$ and 4 . It has typical values in the range $1\text{--}5 \times 10^{12} \text{ W/cm}^2$. Its polarization is along the symmetry axis (z axis) of the system.

The numerical treatment uses the standard techniques of the time-dependent local-density approximation for the cluster electrons and molecular dynamics for Na^+ ions or Ar atoms (TDLDA-MD) as outlined e.g. in [4,18]. The wavefunctions and fields are represented on a grid in coordinate space. The quantum mechanical time stepping is done by the time-splitting method and the molecular dynamics by velocity Verlet. We use absorbing boundary conditions to simulate correctly electron escape.

3 Charge stabilization

The laser irradiation leads to strong ionization of the cluster. An interesting issue is then the Coulomb-stability of the cluster. This has been much studied in the past under the key word ‘‘appearance size’’, the critical size above which clusters of a certain charge state become ultimately stable (i.e. appear in a mass spectrograph), for a review see [27]. It was shown that the value depends sensitively on the excitation mechanism, with ns laser pulses being less favorable, and fs laser pulses as well as fast ion collisions producing significantly lower critical values [28, 29]. For Na clusters, the smallest Na cluster with charge state $Q = 2$ has been observed for Na_{10}^{++} in experiments with laser pulses [30]. The case of free Na_8^{++} , of interest here, is at the edge of stability. Higher charge states $Q \geq 3$, however, lead for sure to immediate Coulomb explosion of free clusters. The interesting question is then how the surrounding Ar environment modifies the charge stability. We will address this question first in terms of asymptotic stability by energetic estimates and then analyze detailed dynamical processes. We will see that the

Ar matrix manages to prevent immediate Coulomb fragmentation for surprisingly high charge states. The strong oscillations of the imprisoned clusters will be analyzed in terms of global shape parameters.

3.1 Stability in principle

TDLDA-MD simulations for free Na_8^{Q+} clusters lead to immediate Coulomb explosion for charge states $Q \geq 3$. The case of Na_8^{++} is at the fringe of stability where small changes in the conditions produce large effects in the results. Monte-Carlo cooling still produces a stable system. The results of dynamical simulations starting from neutral Na_8 and fast ionization depend on the level of approximation. The calculations with axial approximation for the electrons show huge shape oscillations with size varying within a factor of two. Fully three dimensional treatment (without SIC and mere TDLDA) starts in the same manner for the first 5 ps and then ‘‘discovers’’ the Na^+ emission path leading to final Coulomb fragmentation. However, the detailed propagation and the breakup channel depends critically on the initial configuration. Minimal shifts of the ions can lead into totally different directions. It is in any case obvious that the cluster is at least not instantaneously unstable. This observation is corroborated by computing (with the 3D code) the Born-Oppenheimer surfaces in the space of collective deformation (monopole, quadrupole). We find indeed a local minimum for slightly oblate Na_8^{++} surrounded by reaction barriers against fission, as can be seen from Fig. 1. The lowest barrier in that space is about 1 eV. However, the reaction barrier disappears in symmetry breaking directions with single-ion

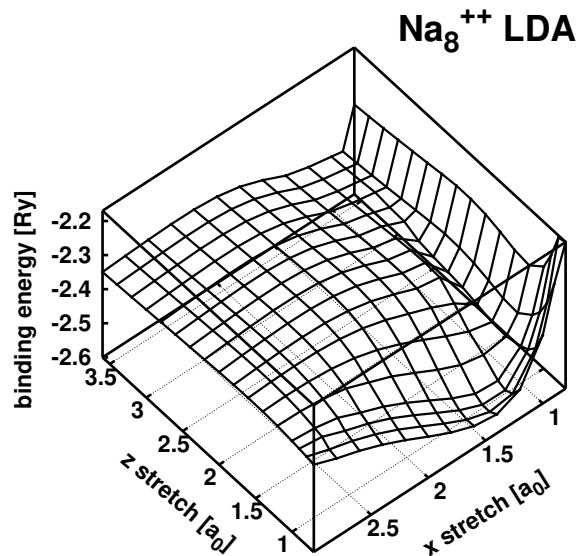


Fig. 1. Born-Oppenheimer surface for free Na_8^{++} in the plane of collective deformations. The energies are shown versus the stretching factor in z and x direction. Three dimensional LDA calculations were used.

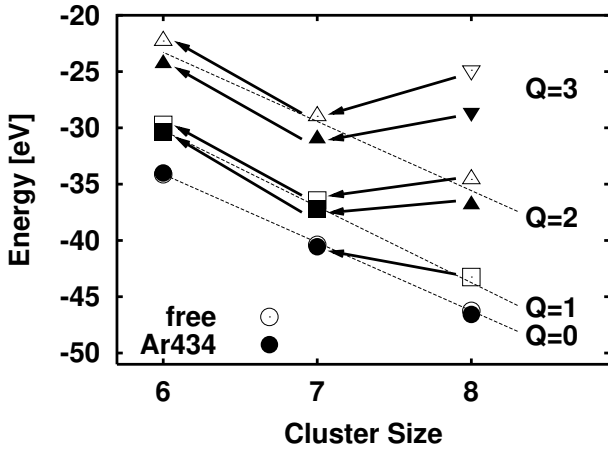


Fig. 2. Binding energies for Na_n^{Q+} clusters, free (open symbols) or embedded in Ar_{434} (filled symbols). The different symbols characterize the charge state: $Q = 0 \leftrightarrow$ circles, $Q = 1 \leftrightarrow$ squares, $Q = 2 \leftrightarrow$ up-triangles, $Q = 3 \leftrightarrow$ down-triangles. The faint dotted lines connect clusters along same charge states Q . The arrows show the energetic path for emission of one Na^+ ion. All clusters have been fully relaxed into their optimal configuration.

escape. The Coulomb excitation by immediate ionization thus produces a metastable state. It requires some time to develop sufficient asymmetry for breakup. The example shows that a case like Na_8^{++} which lies at the limits of stability imposes high demands on the theoretical description. Nonetheless, one can read the result positively: all approaches agree in predicting a long initial period of quasi-stability which is well in the range of experimental observation, e.g. by pump-and-probe techniques assessing the time evolution of cluster shape through the time evolution of the Mie plasmon resonance [31,32,33].

Before proceeding to the dynamical simulations, we want to calibrate our expectations by looking at the asymptotic stability. To that end, we compute the ground-state binding energies of various Na clusters for several charge states. The results for free and embedded clusters are shown in Fig. 2. The steady down-slope of the dotted lines shows that the binding energy for fixed Q increases in almost constant amounts with the number n of Na^+ ions. The energy difference in vertical direction represent the (adiabatic) ionization potentials which naturally increase with increasing charge states. The most interesting part is to look at the decay paths of the highly charged clusters, going along emission of a Na^+ ion (arrows). Down slope means energy gain and thus asymptotic instability. A system may be locally stable for quite a while (see the above discussion). However at long times, the system will find its way to the configuration with lower energy. Free Na_8^{++} is indeed found to be asymptotically unstable. The energy difference shrinks to a negligible amount for embedded Na_8^{++} . This system will then be stable. We see generally that embedding has a stabilizing effect for charged clusters. For example, the case of Na_3^{3+} which was clearly explosive for the free cluster is “downgraded”

to a situation which is comparable to free Na_8^{++} . Energy differences alone however are not fully conclusive for the stability times. These depend also on the phase space of decay channels and on the reaction barriers. The latter are certainly larger for embedded clusters, since a single Na^+ would have to find its way through the closely packed Ar medium.

3.2 Detailed view

Let us now turn towards the analysis of the dynamical scenario following the irradiation of an embedded Na_8 . The initial reaction to laser excitation is exactly the same as we had already observed previously for the more moderate cases [16]. There is a fast direct emission of electrons. The pattern are the same for free and for embedded clusters. The Ar environment does not impose any hindrance, even for the largest system in our sample carrying 1048 Ar atoms. The fast ionization is completed at the end of the pulse, i.e. at 100 fs, and we are left with a cluster in a certain charge state Q depending on the laser intensity. The finite net charge of our test system is related to the finite size of the setup. In a macroscopically large matrix, the electrons would be stuck somewhere within the range of their mean free path. They may even drift very slowly back towards the now attractive cluster, and eventually recombine there. We have simulated that by using reflecting boundary conditions rather than absorbing ones and we find recombination times of the order of several 10 ps. Thus the present scenario should provide a pertinent picture for several ps, the time window studied here.

The Coulomb pressure generated by the almost instantaneous ionization drives the cluster ions apart which, in turn, stir up the Ar atoms. The dominant effect is expansion. Thus a visualization in terms of radial coordinates is most appropriate. This is done in Fig. 3 showing the detailed time evolution for the various charge states and system sizes. The cavity is spacious, leaving a large initial separation of the Na ions from the first shell of Ar atoms. Thus we see for the initial 200 fs a fast expansion/explosion of the cluster almost as in the free case. The expansion is stopped instantaneously if the cluster runs against the repulse Ar core. The stopping radius increases with the charge state Q . After stopping, the cluster turns over into oscillations for a while. The Ar atoms take up the momentum from the stopped ions. That momentum propagates like a sound wave through the Ar medium. The perturbation is strong enough for $Q = 4$ to produce finally a direct emission of Ar atoms when the wave has reached the outmost shell. On the way out, the wave distributes the energy very quickly over all shells exciting them to more or less hefty fluctuations. The Ar amplitudes increase with increasing charge state Q and decreasing system size. The charge dependence is related to the initial amount of Coulomb energy $\propto Q^2$. The size dependence comes from the sharing of energy over the Ar degrees of freedom. More Ar atoms leave less energy per atom and subsequently a smaller amplitude of motion. The Ar matrix appears surprisingly robust for $N = 434$ and larger.

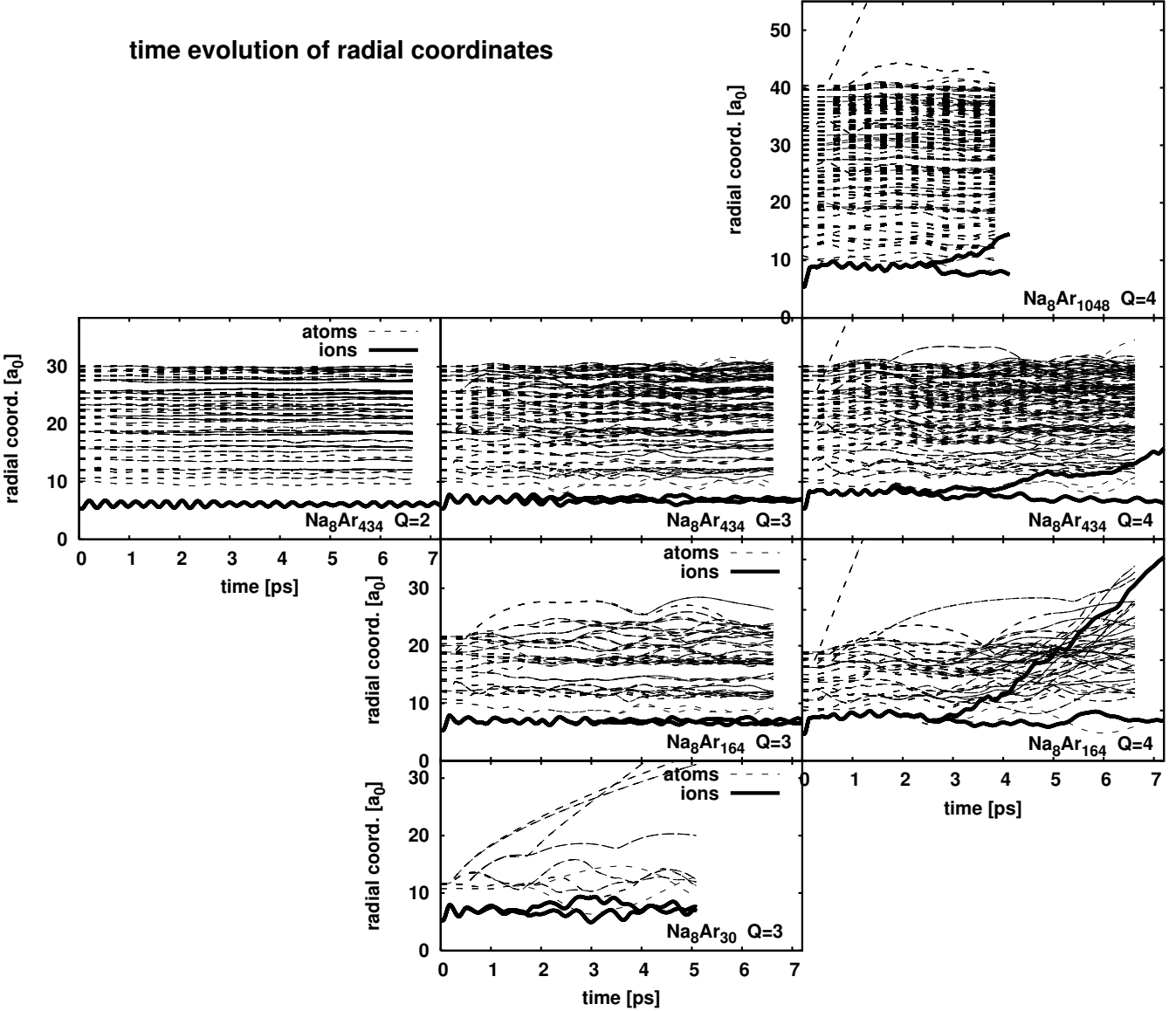


Fig. 3. Time evolution of radial coordinates $r_n = \sqrt{x_n^2 + y_n^2 + z_n^2}$ of ions (heavy lines) and atoms (faint lines) for embedded Na_8 after irradiation with a short laser pulse having $\omega_{\text{laser}} = 2$ eV and \sin^2 envelope with FWHM = 33 fs. The intensity is varied to reach the different final charge stages Q as indicated. The plotting of the Ar atoms is stopped a bit earlier to display more clearly the final status of the Na ions.

Heating suffices for $N = 30$, $Q = 3$ and $N = 164$, $Q = 4$ to induce a steady dissolution of the Ar environment within a few ps. The process starts from the outer shells (mind that melting starts generally at the surface [34]) such that the Na cluster remains still captured by the Ar shells for a long time. The motion of the outmost shell shows also interestingly large excursions in other cases ($N = 164$ at $Q = 3$ and $N = 434$ at $Q = 4$). The high net charge of the total system together with the dipole polarizability of the Ar atoms generates a long-range attractive potential $\propto r^{-4}$ which allows for these large fluctuations of still bound atoms. The stabilization of the cluster appears rather limited for the highest charge state $Q = 4$. At about 4 ps, the cluster expansion revives. It proceeds, however,

at a very slow time scale. One could call that a Coulomb driven diffusion through the medium. Such a process is not visible within the studied time span (up to 10 ps, shown are 7 ps for graphical reasons) for charge state $Q = 3$. It cannot be excluded on a longer time span. However, in any case up to $Q = 4$, we see a temporary stabilization inside the cavity which lasts sufficiently long for an observation.

We can also read off from Fig. 3 a few time scales. The initial Coulomb explosion lasts only for about 200 fs. The distribution of energy over the Ar shells is done within 0.5-0.7 ps. In fact it propagates with the speed of the sound wave which is about $30 a_0/\text{ps}$ for $Q = 3$ and even faster for $Q = 4$. This is close to the velocity of sound in pure Ar, as we will see in the next section. The

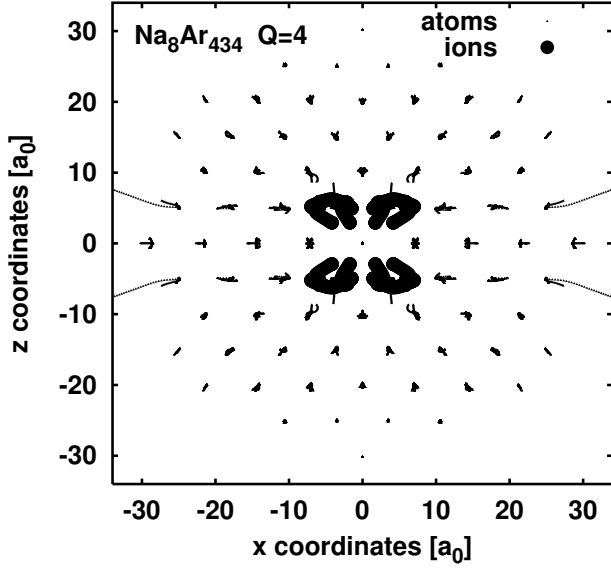


Fig. 4. Trajectories in the x - z -plane for $Q = 4$ and $N = 434$.

temporary stabilization of the cluster lasts about 4 ps for $Q = 4$, a yet unknown longer time for $Q = 3$. The thermal dissolution of the Ar system takes several ps starting from outmost shells.

The instantaneous stopping, the sound wave and the subsequent direct emission of Ar atoms are interesting processes which deserve further inspection. Fig. 4 shows a projection of ionic and atomic trajectories onto the x - z plane (where z denotes the symmetry axis, and laser polarization axis). The ions start with a radial Coulomb explosion, are bent over with little energy loss by about 135° and hit almost head on the next Ar atom. This then triggers the sound wave. The wave is not well visible in coordinate space. It is basically a momentum wave transmitted through small kicks of the atoms. The final kick, however, releases the atom in the last shell for a long travel. All eight ions perform the initial looping similarly and eight Ar atoms are eventually released in that case of $Q = 4$ and $N = 434$.

3.3 Global shape

Complementing information can be gained from characterizing the system through global shape parameters. The leading quantity is the overall extension which can be quantified by the root-mean-square (r.m.s.) radius r . Next important is the quadrupole deformation which we describe by the dimensionless quadrupole moment β_2 . Both observables are defined in detail as

$$r = \sqrt{\frac{1}{p} \sum_{n=1}^p r_n^2} \quad , \quad (12a)$$

$$\beta_2 = \sqrt{\frac{\pi}{5}} \frac{1}{pr^2} \sum_{n=1}^p (2z^2 - x^2 - y^2) \quad . \quad (12b)$$

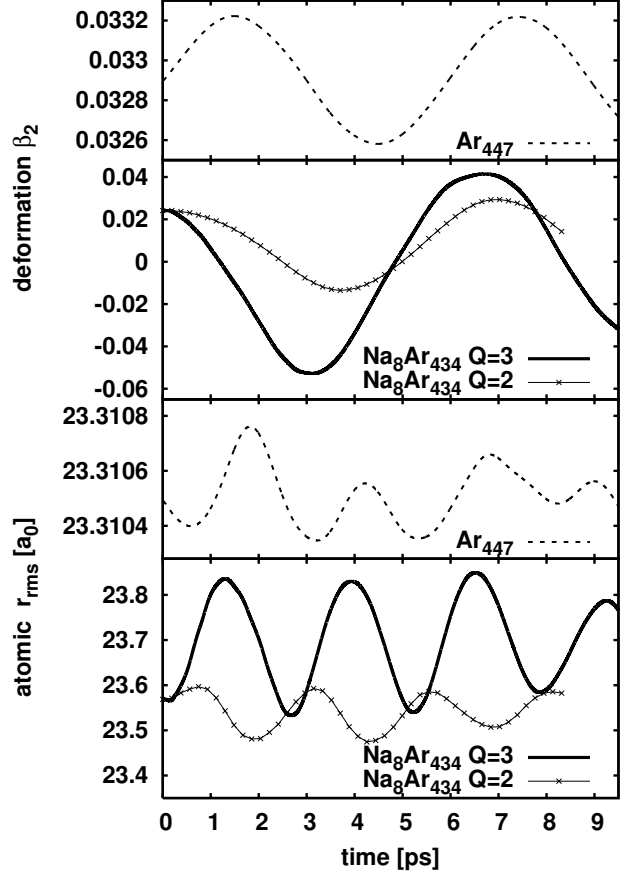


Fig. 5. Time evolution of atomic shape parameters (12), r.m.s. radius r and deformation β_2 , for a pure Ar_{447} cluster and $\text{Na}_8\text{Ar}_{434}$ at two charge states.

These shape parameters are computed for the Na cluster as well as for the Ar system. The sum runs up to $p = 8$ for the Na cluster and up to $p = N$, the number of Ar atoms.

Fig. 5 shows the time evolution of atomic shape parameters for two charge states in Ar_{434} and compares it with the corresponding pure Ar cluster Ar_{447} which contains also the 13 atoms of the cavity. The Ar_{447} was excited by the same laser pulse as for the case $Q = 3$. The laser has a handle on the Ar atoms through their dynamical dipole polarizability. The oscillations have surprisingly much in common. Besides the amplitudes, the pattern are similar and so are the cycle times, for radial oscillations about 2-3 ps and for quadrupole oscillations about 6-7 ps. The large charge at the center of the system seems to change very little on the global properties. The matrix is also in that sense inert. The cleanly developed modes allow to estimate the sound velocity in these large clusters. The radial compression mode corresponds to the longitudinal sound mode in bulk material. Its frequency is $\omega_{\text{vib}} \approx 1.8$ meV. The momentum of the radial wave is $q = \pi/R$ where $R = 30 a_0$ is the cluster radius. The sound velocity is then estimated as $v_{\text{sound}} = \omega_{\text{vib}}/q \approx 30 a_0/\text{ps}$ which is very close to the propagation speed as observed in Fig. 3. The quadrupole mode is a surface mode. Its lower frequency of

about 0.7 meV yields a velocity of 12 a_0 /ps corresponding to a surface sound wave.

The amplitudes are, of course, different for the various cases (note the vertical scales in Fig. 5). The strong laser field has a very small, although visible, effect on the pure cluster. The strong reaction for the composite system is due to the chromophore embedded at the center. This couples strongly to the laser, becomes ionized, and transfers a large portion of its excitation to the Ar surroundings. The strength of the initial excitation (that is, ionization) translates directly into the amplitude of the indirectly triggered oscillations.

Fig. 6 summarizes the time evolution of ionic and atomic shape parameters for a great variety of systems (left column with $N_{\text{Ar}} = 434$ and varying charge Q , right column with $Q = 3$ and varying N_{Ar}). The ionic radii show again the fast stopping. The stopping radius depends strongly on the charge state Q (left lower panel) but seems independent of matrix size (right lower panel). What counts is the first shell of Ar atoms whose radius is the same in all Ar surroundings [15]. We also nicely see the steady oscillations for $Q \leq 3$ and the start of Coulomb diffusion at 4 ps for $Q = 4$. Comparing the ionic r_{rms} for $Q = 2$ and $Q = 3$ (lower left panel), we see that larger Q leads to stronger damping of the ionic oscillations because the ions, coming closer to the Ar atoms, couple more efficiently to the Ar system. The Na^+ -Ar relaxation time which is very long for moderate excitations (see $Q = 2$ here and [16]) shrinks to about 4 ps for $Q = 3$. The effect of system size on the relaxation (right lower panel) is small when comparing $N = 434$ with 164. The case of $N = 30$ is too chaotic to be conclusive.

The effect on the atomic radii (second lower panel in Fig. 6) is related to stopping radius (left) and to system size (right). Larger ionization translates to larger amplitudes up to direct atom emission ($Q = 4$). Smaller system size yields more energy per atom and also increases the amplitudes (right panel). Particularly impressive is the case of $N = 164$ with $Q = 3$. This system shows comparatively huge non-linear fluctuations and is thus at the onset of melting.

The quadrupole moments (upper two panels) behave analogously. The Na ions show a strong initial reaction and then develop in the average a large oblate deformation (negative β_2). The damping again strongly depends on charge state Q and less on system size. The final fragmentation for $Q = 4$ goes clearly to the oblate side. Actually the Coulomb force enhances deformation and we start from the oblate side. That means geometrically that the ions depart preferably orthogonal from the symmetry axis (and thus the laser polarization). The trend to the oblate side carries over to the Ar atoms in unstable situations. Still, the average deformation remains negligible in the stable cases, showing again the inertness of the Ar matrix.

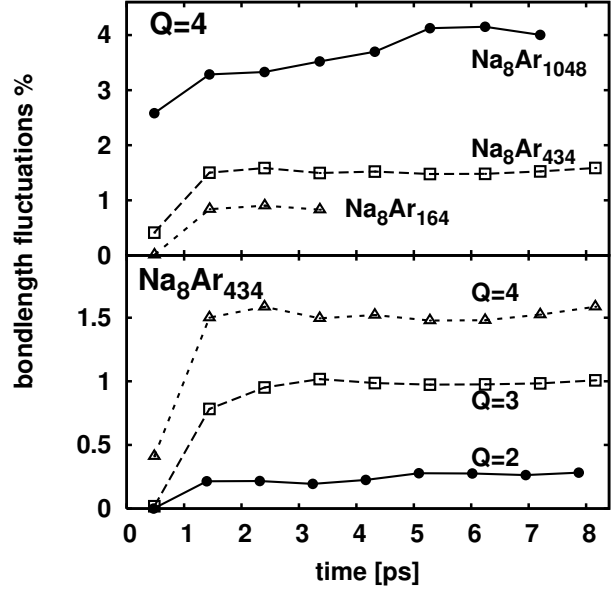


Fig. 7. Time evolution of the bond length fluctuation (13). Lower panel : Case of $\text{Na}_8\text{Ar}_{434}$ at three different charge states. Upper panel : Charge state $Q = 4$ for three different matrix sizes.

3.4 Bond lengths

The shape parameters (12) provide a global measure. A complementing view inside the system is provided by quantifying the bonding structure. It is related to the distances between the Ar atoms. These are fixed in a totally frozen configuration. The temporal fluctuations of the distances help to conclude on the stability of a structure. A convenient measure is the average bond length fluctuation

$$\delta_{\text{bond}} = \frac{2}{N(N-1)} \sum_{i < j} \frac{(\langle r_{ij}^2 \rangle - \langle r_{ij} \rangle^2)^{1/2}}{\langle r_{ij} \rangle} \quad (13)$$

where $\langle \dots \rangle$ is a time-average over a large interval. We use here 1 ps averaging time. The bond length fluctuation is dimensionless, rescaled by the average bond distance. Thus it measures selectively the state of order. A collective deformation (radial expansion, quadrupole deformation) thus does not contribute significantly.

Fig. 7 shows results for the bond length fluctuations. They remain surprisingly small in all cases. At first glance, this seems to contradict the huge spatial fluctuations seen in Fig. 3. Two points are nevertheless to be noted. First, the fluctuations start at the outer shells while the majority of inner Ar atoms remains still better behaved, and second, the bond length fluctuations measure the intrinsic order while being insensitive to global motion. The result indicates that the Ar system stays surprisingly cold in spite of the sometimes hefty reactions. This conclusion will be corroborated by an analysis of the internal temperatures in the following section.

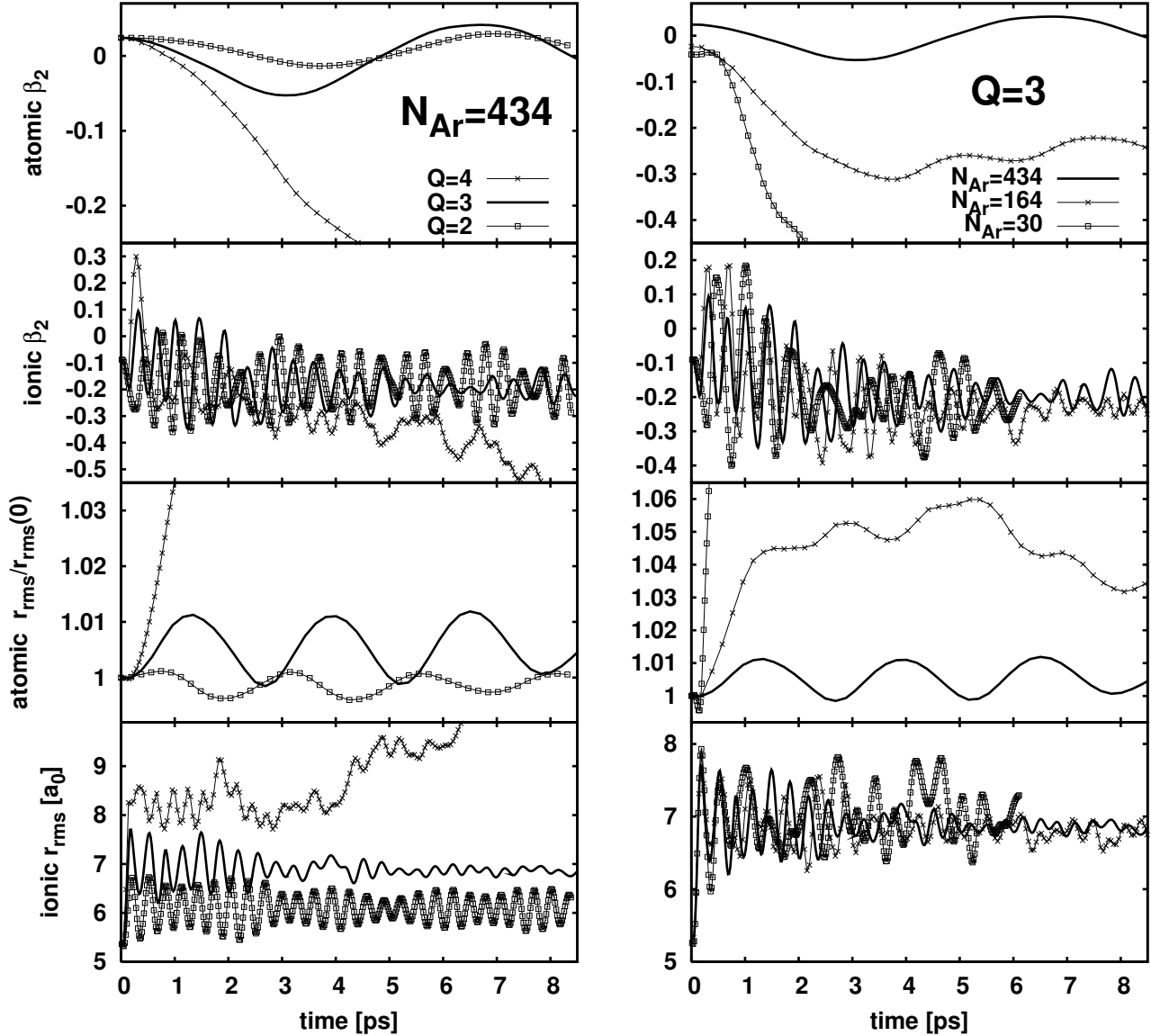


Fig. 6. Time evolution of atomic and ionic shape parameters, Eq. (12), r.m.s. radius r and deformation β_2 , for several test cases in comparison. Left panel : Variation of charge state Q for matrix size $N_{Ar} = 434$. Right panel : Variation of matrix size for charge state $Q = 3$.

4 Energy transfer

Less visible but equally important observables are the various energies in the subsystems and the flow between them. In fact, energy transport and thermalization are most important issues in composite systems, e.g. for analyzing radiation damage in materials [35,36]. The simplest way to characterize the share of energies uses the kinetic energies. These are one-body operators and allow an unambiguous definition for each subsystem, for the cluster electrons, the ions, and the Ar atoms. Fig. 8 shows the ionic and atomic kinetic energies for $Q = 3$ and various matrix sizes. The initial phase is detailed in the left panels. One sees the explosive growth of ionic energies and the sudden stopping with nearly complete energy exchange between ions and atoms. About 2/3 of the initial kinetic energy is kicked

over at once to the first Ar shell. The ions turn to oscillations and the damping of the oscillations, seen in Figs. 3 and 6, leads to a steady reduction of ionic kinetic energy. The further evolution of the atomic kinetic energy stays below the first peak. Part of the initial energy gain is invested into potential energy for spatial rearrangement of atomic positions and dipoles. Something new happens at about 2 ps, particularly for $N = 434$. The kinetic energy increases by about 50%. Part of that energy comes from ionic relaxation. Another part has to stem from further spatial rearrangement into an energetically more favorable configuration. After that, the atomic energy stays almost constant. All further energy transfer processes are too slow to be resolved within simulation time.

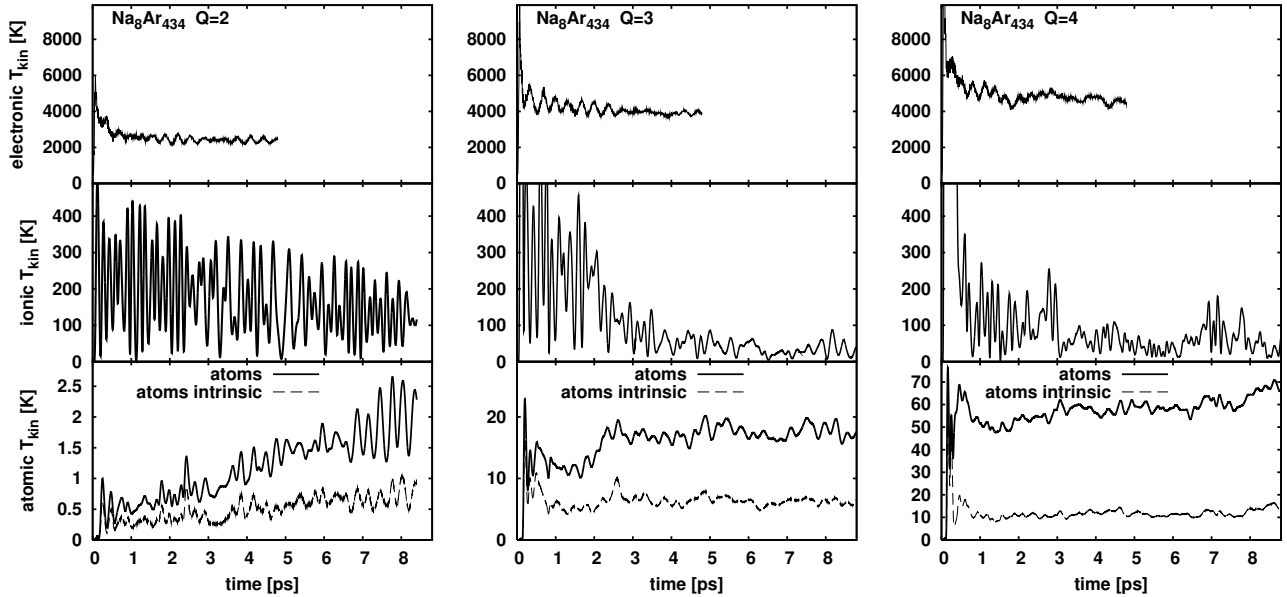


Fig. 9. Time evolution of electronic, ionic and atomic kinetic temperatures for $\text{Na}_8\text{Ar}_{434}$ at three different charge states. For the atoms, we show the temperature from total kinetic energy and from “intrinsic” kinetic energy for comparison (the kinetic energy from collective radial motion is subtracted).

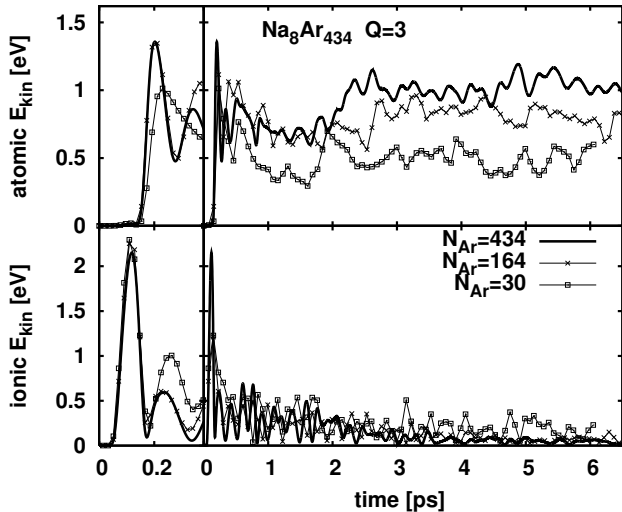


Fig. 8. Time evolution of ionic and atomic kinetic energies for Na_8 in matrices of different size at charge state $Q = 3$. The left panel zooms on the first few 100 fs.

However total energies are not the best measure for internal excitation. Energy per particle is better suited. That leads naturally to the concept of the kinetic temperature $T_{\text{kin}} = 2E_{\text{kin}}/(3N)$. The definition is a bit more involved for the electrons. The kinetic energy as expectation value of wavefunctions contains an unavoidable offset from quantum uncertainty and from the Pauli principle. We subtract that offset, as well as possible collective flow contribution, to define an intrinsic electron temperature, following the procedure described in [18].

The various kinetic temperatures are shown for $N = 434$ and all three charge states in Fig. 9. Note that elec-

trons can use the same scale for the different Q . Their intrinsic temperature grows with Q but less than linearly. That is due to the strong cooling through ionization, see the discussion of Fig. 10 later on. In any case, the electronic temperatures are much higher than any other and there is no sign of relaxation towards the other parts, on the time span explored here. This shows that from a thermal point of view electrons and ions/atoms are, to a large extent, still decoupled. One can conclude that thermal relaxation times seem to be far beyond our analysis. The large electronic temperatures call, in fact, for a description beyond pure mean field. Electron-electron collisions play a role in that regime. These could be included by switching to a semi-classical Vlasov-Uehling-Uhlenbeck description of the electron cloud [17,37]. But long-time semi-classical propagation is extremely hard to stabilize and, as we have seen above, electrons are almost decoupled from ions, thermally speaking. Thus we can neglect that effect for the present study, at least on the time scales explored here.

The ionic temperatures show somewhat larger variation, still fitting almost on the same scale. The initial peak (see lower left panel in Fig. 8) is not fully shown here. It grows with a rate between linear and quadratic in Q . The further evolution shows the reverse trend. The kinetic energies shrink the faster the higher Q . That is due to the increasing coupling to the first Ar shell which accelerates the energy exchange to the Ar system.

Totally different temperature scales are required for the Ar matrix. Two effects cooperate here: The ionic kinetic energy grows with Q and the coupling to the Ar is strongly enhanced with the increasing ionic stopping radius, see lower left panel of Fig. 6. The case of $Q = 2$ does not show the abrupt stopping and thus does not have the large initial jump in energy. The temperature rather

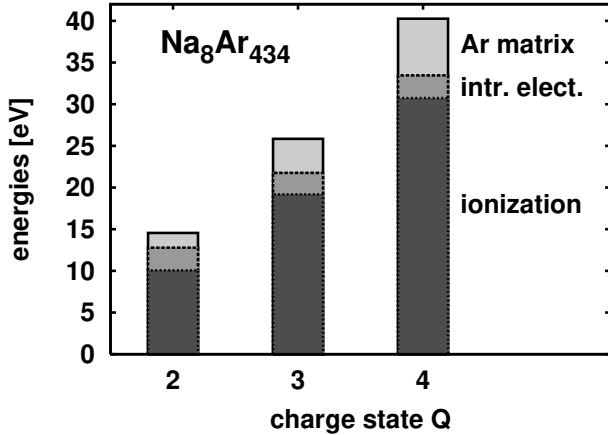


Fig. 10. Distribution of the energy initially absorbed from the laser over the various reaction channels : “ionization” stands for the energy used up to reach the ionization stage Q , “intr. elect.” stands for the intrinsic electronic kinetic energy left in the remaining electron cloud, “Ar matrix” stands for the kinetic and potential energy stored in the Ar matrix after relaxation (Na^+ ions have then only a very small share).

grows steadily in relation to the equally steady cooling of the ionic cloud. The relaxation time for the thermalization is of order of 10 ps. That relaxation time drops to 2-3 ps for the larger Q with their more intimate Na^+ -Ar coupling. Moreover, most of the energy transfer is concentrated in the stopping and comparatively little is left for the subsequent energy exchange. Within the resolution of the results, we can state that Na^+ -Ar thermalization is achieved after 4 ps for $Q = 3$. The energy continues to increase for $Q = 4$. That is due to the Coulomb diffusion which converts steadily potential into kinetic energy.

The results from section 3 show a large amount of collective motion in radial direction and in quadrupole deformation. That part of motion is still included in the total atomic kinetic energy. In order to single out the irregular part corresponding to truly intrinsic excitation, we have computed the collective kinetic energy contained in the radial oscillations (the slower quadrupole part contributes very little) and subtracted it to obtain an intrinsic kinetic energy. The corresponding kinetic temperature is also shown as the curves labeled “atoms intrinsic” in the lower panels of Fig. 9. The collective part is always the largest portion and even dominates by far for $Q \geq 3$. The minor part is left for intrinsic motion. That explains the findings from the bond lengths in Fig. 7 which show very little perturbation of the internal structure of the Ar system. In spite of the huge amounts of energy flowing around, that structure persists astonishingly robust.

Finally Fig. 10 shows the distribution of the excitation energy initially induced by the laser. The total height stands for the excitation energy. Of course, it increases with increasing intensity and subsequently increasing charge state. This net investment grows a bit faster than linear. Earlier experience with free clusters shows that a major cooling mechanism is electron emission [38,39]. We have

estimated that for the present case by integrating the ionization potentials (IP) along the ionization curve and by computing the IP as a function of charge for fixed ionic configuration. The results in Fig. 10 prove that indeed the by far dominant portion of energy is carried away with the directly emitted electrons. That removes typically 80% of the laser energy. The next two large contributors are the intrinsic electronic energy and the final energy of the Ar atoms (which was, to a large extent, initially ionic kinetic energy). The share depends strongly on the charge state. Very little is left for the Ar atoms at $Q = 2$ while they gather almost equal share for $Q = 4$. Here we have to keep in mind that the energy balance in Fig. 10 represents the status at the end of the simulation, i.e. at 6 ps. Final full thermalization (if reached before dissolution of the system) will give the kinetic energy of electrons, ions and atoms, with a thermal share proportional to the number of particles in each subsystem. We have order of 8 electrons and ions but much more atoms. Thus the Ar system will acquire finally almost all residual energy which amounts to about 3-6 eV, corresponding to a heating of about 50-100 K.

5 Conclusions

We have analyzed the laser-induced dynamics of a Na_8 cluster embedded in an Ar matrix. We have used a hierarchical model with a detailed quantum-mechanical treatment of the clusters electron cloud and a classical description of the Na^+ ions as well as of the surrounding Ar atoms whereby we include the Ar dipole moments to account for the dynamical polarizabilities. The Ar matrix is approximated by a large Ar cluster covering several shells of atoms. To distinguish finite size effects, we have used different sizes from $N = 30$ to 1048 Ar atoms. The test cases provide several interesting aspects : They are by construction a model for a cluster embedded in a rare gas matrix, they display also interesting features specific for a finite composite, and they are prototypes of a chromophore in an else-wise inert material. For the excitation mechanism, we consider irradiation by a short 33 fs laser pulse with intensity of about $10^{12} \text{W}/\text{cm}^2$.

It was found in earlier studies of structure and mild excitations that the Ar matrix induces only very small perturbations of the cluster properties. That remains true for the electronic dynamics in the more violent regime. However, the now released large amplitude motion of the cluster ions interferes with the atomic cage. This produces dramatic differences of the cluster dynamics as compared with the free case. The (meta-)stability of charged clusters is much enhanced; even a Na_8^{4+} cluster remains bound for about 4 ps, and lower charge states much longer. The Coulomb explosion of the highly ionized cluster is abruptly stopped by the first shell of Ar atoms and most of ionic kinetic energy is transferred to the Ar shell within a few 10 fs. The transferred energy is then spread very quickly by a sound wave all over the Ar matrix. Subsequent relaxation and rearrangement processes between ions and atoms proceed at a time scale of several ps. The Coulomb

instability takes over within that time span for $Q = 4$ and drives a slow Coulomb-driven diffusion of Na^+ ions through the Ar medium. All processes related to shape evolution within that time scale are in reach of experimental observation by pump-and-probe analysis using the cluster surface plasmon as handle.

We have also analyzed the energy balance. The time scales for energy transfer confirm the findings for the ionic-atomic relaxation as deduced from shape analysis. The electron cloud adds by far the most efficient energy loss through direct ionization during laser impact. And even after large energy outflow with the emitted electrons, a large part of excitation energy remains kept in internal energy of the electrons because the thermal (i.e. non-collective) coupling of electrons to ions and atoms is extremely weak. The small remaining fraction of excitation energy goes through Coulomb energy (charging), kinetic energy of Na^+ ions (Coulomb explosion), quickly to the Ar system. In spite of the small amount of initial laser energy finally transmitted to the Ar matrix, the Na cluster as chromophore pumps orders of magnitude more energy into the system as a pure Ar cluster would be able to extract from the same laser pulse.

This work was supported by the DFG (RE 322/10-1), the french-german exchange program PROCOPE, the CNRS Programme "Matériaux" (CPR-ISMIR), Institut Universitaire de France, a Bessel-Humboldt prize and a Gay-Lussac prize.

References

1. W.A. de Heer, Rev. Mod. Phys. **65**, 611 (1993)
2. M. Brack, Rev. Mod. Phys. **65**, 677 (1993)
3. U. Kreibig, M. Vollmer, *Optical Properties of Metal Clusters*, Vol. 25 (Springer Series in Materials Science, 1993)
4. P.G. Reinhard, E. Suraud, *Introduction to Cluster Dynamics* (Wiley, New York, 2003)
5. C. Mayer, R. Palkovits, G. Bauer, T. Schalkhammer, J. Nanoparticle Res. **3**, 361 (2001)
6. B. Dubertret, P. Skourides, D.J. Norris, V. Noireaux, A.H. Brivanlou, A. Libchaber, Science **298**, 1759 (2002)
7. W. Harbich, S. Fedigro, J. Buttet, Z. f. Physik D **26**, 138 (1993)
8. T. Diederich, J. Tiggesbäumker, K.H. Meiwes-Broer, J. Chem. Phys. **116**, 3263 (2002)
9. H. Häkkinen, M. Manninen, J. Chem. Phys. **105**, 10565 (1996)
10. U.L. M. Moseler, H. Häkkinen, Physical Review Letters **89**, 176103 (2002)
11. C. Sieber, J. Buttet, W. Harbich, C. Flix, R. Mitri, V. Bonai-Kouteck, Phys. Rev. A **70**, 041201 (2004)
12. N. Gresh, O. Parisel, C. Giessner-Prettre, THEOCHEM **458**, 27 (1999)
13. A. Nasluzov, K. Neyman, U. Birkenheuer, N. Rösch, J. Chem. Phys. **115**, 17 (2001)
14. B. Gervais, E. Giglio, E. Jaquet, A. Ipatov, P.G. Reinhard, E. Suraud, J.Chem.Phys. **121**, 8466 (2004)
15. F. Fehrer, P.G. Reinhard, E. Suraud, E. Giglio, B. Gervais, A. Ipatov, Appl. Phys. A **82**, 151 (2005)
16. F. Fehrer, P.G. Reinhard, E. Suraud, Appl. Phys. A **82**, 145 (2006)
17. F. Fehrer, M. Mundt, P.G. Reinhard, E. Suraud, Ann. Phys. (Leipzig) **14**, 411 (2005)
18. F. Calvayrac, P.G. Reinhard, E. Suraud, C.A. Ullrich, Phys. Rep. **337**, 493 (2000)
19. B.G. Dick, A.W. Overhauser, Phys. Rev. **112**, 90 (1958)
20. F. Dupl ae, F. Spiegelmann, J. Chem. Phys. **105**, 1492 (1996)
21. G.R. Ahmadi, J. Alml of, J. Roegen, Chem. Phys. **199**, 33 (1995)
22. M. Gross, F. Spiegelmann, J. Chem. Phys. **108**, 4148 (1998)
23. M.B. El Hadj Rhouma, H. Berriche, Z.B. Lakhdar, F. Spiegelman, J. Chem. Phys. **116**, 1839 (2002)
24. B. Gervais, E. Giglio, P.G. Reinhard, E. Suraud, Phys. Rev. A **71**, 015201 (2004)
25. C. Legrand, E. Suraud, P.G. Reinhard, J. Phys. B **35**, 1115 (2002)
26. K. Andrae, A. Pohl, P.G. Reinhard, C. Legrand, M. Ma, E. Suraud, in *Progress in Nonequilibrium Green's Functions II*, edited by M. Bonitz, D. Semkat (World Scientific, Singapore, 2003), p. 28
27. U. N aher, S. Bj ornholm, S. Frauendorf, F. Garcias, C. Guet, Phys. Rep. **285**, 245 (1997)
28. G.E. Ntamack, B.A. Huber, F. Chandezon, M.G.K. Njock, C. Guet, J. Phys. B **35**, 2729 (2002)
29. P.G. Reinhard, E. Suraud, Int. J. Mol. Sci. **1**, 92 (2000)
30. C. Schmitt, C. Ellert, M. Schmidt, H. Haberland, zphd **42**, 145 (1997)
31. K. Andrae, P.G. Reinhard, E. Suraud, J. Phys. B **35**, 1 (2002)
32. K. Andrae, P.G. Reinhard, E. Suraud, Phys. Rev. Lett. **92**, 173402 (2004)
33. T. D oppner, T. Fennel, P. Radcliffe, J.T. und K-H Meiwes-Broer, Eur. Phys. J. D **36**, 165 (2005)
34. H. Loewen, T. Beier, H. Wagner, Europhys. Lett. **9**, 791 (1989)
35. M.Y. Niv, M. Bargheer, R.B. Gerber, J. Chem. Phys. **113**, 6660 (2000)
36. M. Bargheer, M. Guhr, N. Schwentner, J. Chem. Phys. **117**, 5 (2002)
37. E. Giglio, P.G. Reinhard, E. Suraud, J. Phys. B **34**, 1253 (2001)
38. F. Calvayrac, A. Domsps, P.G. Reinhard, E. Suraud, C.A. Ullrich, Euro. Phys. J. D **4**, 207 (1998)
39. P.G. Reinhard, F. Calvayrac, C. Kohl, S. K ummel, E. Suraud, C.A. Ullrich, M. Brack, Euro. Phys. J. D **9**, 111 (1999)